

First measurements of the absolute branching fraction of $\Lambda_c(2625)^+ \rightarrow \Lambda_c^+ \pi^+ \pi^-$ and upper limit on $\Lambda_c(2595)^+ \rightarrow \Lambda_c^+ \pi^+ \pi^-$

M. Ablikim *et al.**
(BESIII Collaboration)

 (Received 21 January 2024; revised 16 March 2024; accepted 26 April 2024; published 5 June 2024)

The absolute branching fraction of the decay $\Lambda_c(2625)^+ \rightarrow \Lambda_c^+ \pi^+ \pi^-$ is measured for the first time to be $(50.2 \pm 5.7_{\text{stat}} \pm 3.5_{\text{sys}})\%$ with 368.48 pb^{-1} of e^+e^- collision data collected by the BESIII detector at the center-of-mass energies of $\sqrt{s} = 4.918$ and 4.950 GeV . Although the central value of the result is lower than the theoretical prediction of 67%, obtained from isospin symmetry, they are consistent taking the uncertainties into account. This is the first absolute branching fraction measurement for $\Lambda_c(2625)^+$ since it was found. This measurement is necessary to obtain the coupling constants for the transitions between s -wave and p -wave charmed baryons in heavy hadron chiral perturbation theory. In addition, we search for the decay $\Lambda_c(2595)^+ \rightarrow \Lambda_c^+ \pi^+ \pi^-$. No significant signal is observed, and the upper limit on its branching fraction is determined to be 85.0% at the 90% confidence level.

DOI: [10.1103/PhysRevD.109.112007](https://doi.org/10.1103/PhysRevD.109.112007)

I. INTRODUCTION

In recent years, a rich mass spectrum of excited charmed baryons has been discovered [1–5]. Identifying their quantum numbers and understanding their properties are important to study the dynamics of the light quarks in the environment of a heavy quark. The strong decays of charmed baryons are most conveniently described by heavy hadron chiral perturbation theory (HHChPT), in which heavy quark symmetry and chiral symmetry are incorporated [6,7]. The chiral Lagrangian involves several coupling constants for transitions between s -wave and p -wave charmed baryons, referred to as h_2 to h_{15} [8,9]. Among these, h_2 and h_8 can be determined from the strong decays of $\Lambda_c(2595)^+$ and $\Lambda_c(2625)^+$ [1]. These coupling constants are critical to describe the charmed baryon spectrum and make predictions of decays into other charmed baryons. However, so far, the strong decays of $\Lambda_c(2595)^+$ and $\Lambda_c(2625)^+$ are poorly known due to the scarcity of experimental data [2]. The existing determinations of h_2 and h_8 are based on the measured decay widths of $\Lambda_c(2595)^+$ and $\Lambda_c(2625)^+$. Since the width of $\Lambda_c(2625)^+$ is nearly zero [2,5], only the upper limit on h_8 is provided. Precise measurements of the branching fractions of the strong decays of $\Lambda_c(2595)^+$ and $\Lambda_c(2625)^+$ are important to determine h_2 and h_8 .

In the quark model, $\Lambda_c(2595)^+$ and $\Lambda_c(2625)^+$ are the lowest-lying excited states of Λ_c^+ having spin parities of $1/2^-$ and $3/2^-$, respectively, and are the degenerate pair of the p -wave state [1]. Currently, all observed decay modes are measured relative to the dominant hadronic transitions, either $\Lambda_c(2595)^+ \rightarrow \Lambda_c^+ \pi^+ \pi^-$ or $\Lambda_c(2625)^+ \rightarrow \Lambda_c^+ \pi^+ \pi^-$ [3,4]. However, the absolute branching fractions of these $\pi^+ \pi^-$ transitions have until now never been measured experimentally. Assuming isospin symmetry, the ratio between the branching fractions of $\pi^+ \pi^-$ and $\pi^0 \pi^0$ transitions is 2:1, which is the basis for the branching fractions of various strong $\Lambda_c(2595)^+$ and $\Lambda_c(2625)^+$ decays quoted by the Particle Data Group (PDG) [2]. However, isospin symmetry in these processes has not been verified by any experimental measurement. In Ref. [10], a mechanism called the *threshold effect* to take into account the limited transition phase space in these strong decays was proposed. It would break the 2:1 relation between $\pi^+ \pi^-$ and $\pi^0 \pi^0$ transitions in $\Lambda_c(2595)^+$ decay. Furthermore, this mechanism is sensitive to the coupling constants [1,10], and the measurements of their branching fractions are crucial to determine their coupling constants.

In addition, the internal structure of $\Lambda_c(2595)^+$ and $\Lambda_c(2625)^+$ have received much attention since the discoveries of these two baryons. Significantly, different decay properties of $\Lambda_c(2595)^+$ and $\Lambda_c(2625)^+$ are observed in experiments [3,4,11–14]. One example is the decay width: while being approximately 2.6 MeV in the case of $\Lambda_c(2595)^+$, it is smaller than 1 MeV for $\Lambda_c(2625)^+$ [2]. In addition, the $\Lambda_c(2595)^+$ is located at the $\Sigma_c \pi$ mass threshold, and predominantly decays through the intermediate state Σ_c to the hadronic final states $\Lambda_c^+ \pi \pi$, where

*Full author list given at end of the article.

Published by the American Physical Society under the terms of the [Creative Commons Attribution 4.0 International license](https://creativecommons.org/licenses/by/4.0/). Further distribution of this work must maintain attribution to the author(s) and the published article's title, journal citation, and DOI. Funded by SCOAP³.

Σ_c represents the isospin triplet Σ_c^0 , Σ_c^+ , and Σ_c^{++} . However, the $\Lambda_c(2625)^+$ decays into Σ_c are highly suppressed. Exotic features, such as a molecule-like state rather than a conventional three-quark structure, have been proposed as explanations for the difference [15–18]. Other interpretations include dynamically generated meson-baryon states [17], analogous to the case of $\Lambda(1405)$ and $\Lambda(1520)$ [19,20], or a state with large pentaquark components [18].

In this paper, we report the first measurement of the absolute branching fraction of $\Lambda_c(2625)^+ \rightarrow \Lambda_c^+ \pi^+ \pi^-$ and the upper limit on $\Lambda_c(2595)^+ \rightarrow \Lambda_c^+ \pi^+ \pi^-$, obtained from the processes of $e^+e^- \rightarrow \bar{\Lambda}_c^- \Lambda_c(2595)^+$ and $\bar{\Lambda}_c^- \Lambda_c(2625)^+$. We use the data collected with the BESIII at center-of-mass (c.m.) energies of 4.918 and 4.950 GeV [21]. The integrated luminosities of the data samples at 4.918 GeV are 208.1 and 160.4 pb^{-1} [22], respectively. Throughout this paper, unless explicitly stated, charge-conjugate modes are implicitly included.

II. BESIII DETECTOR

Details about the design and performance of the BESIII detector can be found in Ref. [23]. Simulated samples are produced with GEANT4-based [24] Monte Carlo (MC) software, which includes a full implementation of the detector geometry and response [25] of the BESIII detector. The simulations are used to determine the efficiency of the detector and the reconstruction, and to estimate the background. The inclusive MC sample, which consists of $\Lambda_c^+ \bar{\Lambda}_c^-$ events, $D_{(s)}$ production, ψ states produced in initial-state radiation processes, and continuum processes $e^+e^- \rightarrow q\bar{q}$ ($q = u, d, s$), is generated to estimate the potential background. Here, all the known decay modes of charmed hadrons and charmonia are modeled with EvtGen [26,27] using branching fractions taken from the PDG [2], while the remaining unknown decays are modeled with LundCharm [28,29]. Final-state radiation from charged final-state particles is incorporated using PHOTOS [30]. The processes of these hadron productions are referred to as inclusive background hereafter.

III. METHODOLOGY AND MC SIMULATION

To determine the branching fractions, the approach contains two steps. The first is the determination of the total yields for $\Lambda_c(2595)^+$ or $\Lambda_c(2625)^+$, N_{tag} , which follows the same method as in Ref. [31] by using the productions $e^+e^- \rightarrow \bar{\Lambda}_c^- \Lambda_c(2595)^+$ and $\bar{\Lambda}_c^- \Lambda_c(2625)^+$. Three hadronic decay modes ($pK^-\pi^+$, pK_S^0 , and $\Lambda\pi^+$) are used to reconstruct the Λ_c^+ signal, denoted as ‘‘tagged Λ_c^+ ’’ hereafter, and the candidates for $\Lambda_c(2595)^+$ and $\Lambda_c(2625)^+$ are studied with the recoiling mass from the tagged Λ_c^+ . The second step is the determination of signal events for $\Lambda_c(2595)^+$ or $\Lambda_c(2625)^+ \rightarrow \Lambda_c^+ \pi^+ \pi^-$, N_{sig} , by further selecting candidates for $\bar{\Lambda}_c^-$, π^+ and π^- particles. Finally, the branching fractions are calculated as

$$\mathcal{B} = \frac{N_{\text{sig}} \cdot \sum_i \mathcal{B}_{\text{tag}}^i \epsilon_{\text{tag}}^i}{N_{\text{tag}} \cdot \sum_i \mathcal{B}_{\text{tag}}^i \epsilon_{\text{sig}}^i}, \quad (1)$$

where i represents each reconstruction mode of the tagged Λ_c^+ , and $\mathcal{B}_{\text{tag}}^i$ labels their branching fractions. The ϵ_{tag}^i and ϵ_{sig}^i are the efficiencies of determining the total yields N_{tag} and signal yields N_{sig} , respectively.

To select signal events for $\Lambda_c(2595)^+$ and $\Lambda_c(2625)^+ \rightarrow \Lambda_c^+ \pi^+ \pi^-$, a partial reconstruction method is used, where the Λ_c^+ , π^+ and π^- are reconstructed together with another unreconstructed $\bar{\Lambda}_c^-$, as demonstrated in Fig. 1. The Λ_c^+ , which decays into the three hadronic modes, may come from the e^+e^- collision, as in Fig. 1(a), or from the decay of the $\Lambda_c(2595)^+$ or $\Lambda_c(2625)^+$, as in Fig. 1(b). The process in Fig. 1(a) is referred to as S_{bachelor} and the one in Fig. 1(b) as S_{daughter} .

The signal MC samples are generated corresponding to the two processes, separately, for the two c.m. energies using the generator KKMC [32] incorporating initial-state radiation effects and the beam energy spread. The $\bar{\Lambda}_c^-$ in both processes is required to decay into any allowed final states. The line shapes of $e^+e^- \rightarrow \bar{\Lambda}_c^- \Lambda_c(2595)^+$ and $\bar{\Lambda}_c^- \Lambda_c(2625)^+$ cross sections in the production for signal MC samples are obtained from the measurements by BESIII [31] and the amplitudes of $e^+e^- \rightarrow \bar{\Lambda}_c^- \Lambda_c(2595)^+$ and $\bar{\Lambda}_c^- \Lambda_c(2625)^+$ follow the angular distributions measured in Ref. [31]. In addition, the signal MC samples for the charge-conjugate partners are also produced for processes S_{bachelor} and S_{daughter} , respectively, where the $\bar{\Lambda}_c^-$ is reconstructed with the three tag modes $\bar{p}K^+\pi^-$, $\bar{p}K_S^0$, and $\bar{\Lambda}\pi^-$, and the Λ_c^+ is required to decay into any allowed final states.

IV. EVENT SELECTIONS

Charged tracks detected in the helium-based multilayer chamber (MDC) are required to be within a polar angle (θ)

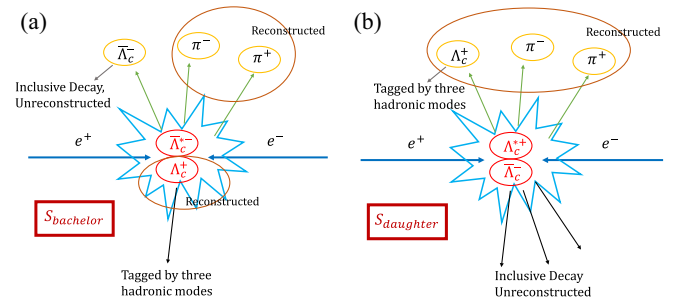


FIG. 1. The signal processes and the partial reconstruction method are schematically presented. (a) The figure corresponds to the S_{bachelor} process where the tagged Λ_c^+ comes directly from the e^+e^- collision and is reconstructed by the three hadronic decay modes. (b) This corresponds to the S_{daughter} process, where the tagged Λ_c^+ comes from the decays of the Λ_c^{*+} , which refers to either $\Lambda_c(2595)^+$ or $\Lambda_c(2625)^+$.

range of $|\cos\theta| < 0.93$, where θ is defined with respect to the z axis, which is the symmetry axis of the MDC. The distance of closest approach for charged tracks that do not come from a Λ or K_S^0 decay are required to be within ± 10 cm along the z axis and 1 cm in the plane perpendicular to the beam. Particle identification (PID) is implemented by combining measurements of the specific ionization energy loss in the MDC (dE/dx) and the time-of-flight (TOF) between the interaction point and the dedicated TOF detector system. Each charged track is assigned a particle type of pion, kaon or proton, according to which assignment has the highest probability. For the mode $\Lambda_c^+ \rightarrow pK^-\pi^+$, a vertex fit is performed to each $pK^-\pi^+$ combination candidate, and the refitted momenta are used in the further study.

Candidates for K_S^0 and Λ are reconstructed by their dominant modes $K_S^0 \rightarrow \pi^+\pi^-$ and $\Lambda \rightarrow p\pi^-$, respectively, where the charged tracks are required to have distances of closest approach to the interaction point that are within ± 20 cm along the z axis. For the Λ decay, the PID requirement is applied to the proton candidate, but not to the charged pion. A secondary vertex fit is performed to each K_S^0 or Λ candidate, and the refitted momenta are used in the further analysis. A K_S^0/Λ candidate requires the χ^2 of the secondary vertex fit to be less than 100. Furthermore, the decay vertex is required to be separated from the interaction point by a distance of at least twice the fitted vertex resolution, and the invariant mass to be within $(0.487, 0.511)$ GeV/c^2 for $\pi^+\pi^-$ and $(1.111, 1.121)$ GeV/c^2 for $p\pi^-$.

In the first step of determining the total yields N_{tag} , all combinations for each decay mode are kept, and their invariant mass distributions are shown in Fig. 2. The tagged Λ_c^+ candidates are required to fall inside the range $(2.27, 2.30)$ GeV/c^2 . The distributions of the recoiling mass from the tagged Λ_c^+ , $M_{\text{recoil}}^{\text{tag}}(\Lambda_c^+)$, are shown in Figs. 4(a) and 4(b) by combining the three modes. There are two components to the signal at each energy, depending on whether the tagged Λ_c^+ originated from the e^+e^- collision directly or from the decay of either $\Lambda_c(2595)^+$ or $\Lambda_c(2625)^+$. If from the e^+e^- collision directly, narrow resonances $\Lambda_c(2595)^+$ and $\Lambda_c(2625)^+$ are observed at two energy points $\sqrt{s} = 4.918$ and 4.950 GeV, from the processes of $e^+e^- \rightarrow \Lambda_c^+\bar{\Lambda}_c(2595)^-$ and $e^+e^- \rightarrow \Lambda_c^+\bar{\Lambda}_c(2625)^-$, respectively. However, if from the decay of either $\Lambda_c(2595)^+$ or $\Lambda_c(2625)^+$, the $\Lambda_c(2595)^+$ and $\Lambda_c(2625)^+$ from the processes $e^+e^- \rightarrow \bar{\Lambda}_c^-\Lambda_c(2595)^+$ and $\bar{\Lambda}_c^-\Lambda_c(2625)^+$ distribute broadly under the resonances. The combined signal shapes are displayed in Figs. 4(a) and 4(b).

In the second step of determining the N_{sig} , in addition to the tagged Λ_c^+ , a $\pi^+\pi^-$ pair is selected by imposing the same criteria as for the charged pion in the mode $\Lambda_c^+ \rightarrow pK^-\pi^+$. A vertex fit is performed to the π^+ and π^- candidates, and the refitted momenta are retained in the further analysis. In the signal processes, there exists another

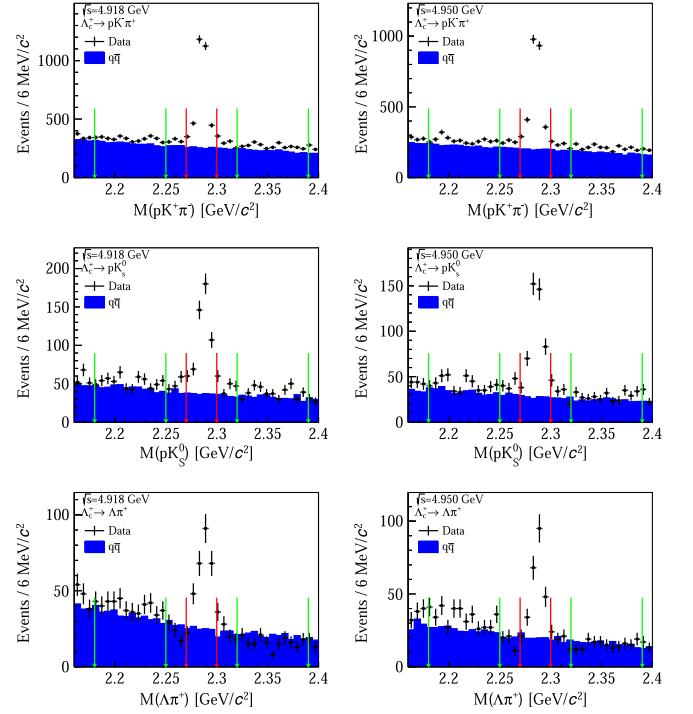


FIG. 2. The distributions of invariant masses of the tagged Λ_c^+ candidates for $\sqrt{s} = 4.918$ (left) and 4.950 GeV (right). The region between the red arrows in the middle is the signal region $(2.270, 2.310)$ GeV/c^2 and the regions between two neighbor green arrows are the sideband regions $(2.180, 2.250)$ and $(2.320, 2.390)$ GeV/c^2 .

$\bar{\Lambda}_c^-$ besides the tagged Λ_c^+ and the $\pi^+\pi^-$ pair. To improve the detection efficiency, the $\bar{\Lambda}_c^-$ is unreconstructed and considered to be a missing particle. If there is more than one combination in an event, we select only the best combination that gives the minimum $|\Delta M|$,

$$\Delta M = \sqrt{\left[2E_{\text{beam}} - \left(\sum_i E_i\right)\right]^2 - \left(\sum_i \vec{p}_i\right)^2} - m_{\Lambda_c}^{\text{PDG}}, \quad (2)$$

where E_{beam} is the beam energy and $m_{\Lambda_c}^{\text{PDG}}$ is the Λ_c^+ nominal mass, E_i and \vec{p}_i represent the energy and momentum, respectively, and i labels the tagged Λ_c^+ , π^+ , and π^- particles. To suppress inclusive background contamination, ΔM , shown in Fig. 3, is required to be greater than -0.02 GeV, which keeps more than 97% of signal. With all the selection criteria, the invariant mass distributions of the $\Lambda_c^+\pi^+\pi^-$ system, $M(\Lambda_c^+\pi^+\pi^-)$, and the Λ_c^+ recoiling mass, $M_{\text{recoil}}^{\text{sig}}(\Lambda_c^+)$, are obtained as shown in Figs. 4(c), 4(d), 4(e) and 4(f). The resonance $\Lambda_c(2625)^+$ appears in both the $M(\Lambda_c^+\pi^+\pi^-)$ and the $M_{\text{recoil}}^{\text{sig}}(\Lambda_c^+)$ distributions at each energy point, corresponding to the processes S_{daughter} and S_{bachelor} , respectively. However, due to quite low detection efficiencies for the low-momentum π^+ and π^- , $\Lambda_c(2595)^+$

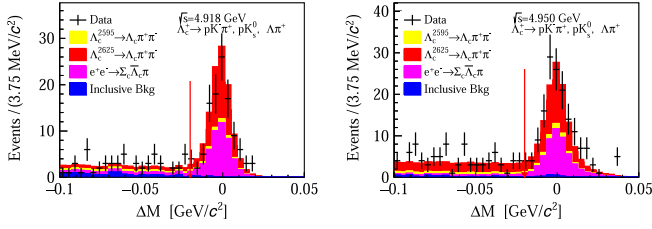


FIG. 3. The distributions of ΔM for $\sqrt{s} = 4.918$ (left) and 4.950 GeV (right). The red arrows indicate the cut $\Delta M > -0.02$ GeV/ c^2 .

is not observed. Here, as for Figs. 4(a) and 4(b), the $M_{\text{recoil}}^{\text{sig}}(\Lambda_c^+)$ signal shapes in Figs. 4(e) and 4(f) have two components depending on whether the Λ_c^+ comes from the e^+e^- collision or from $\Lambda_c(2625)^+$. Also the $M(\Lambda_c^+\pi^+\pi^-)$ signal shapes in Figs. 4(c) and 4(d) have two components. There is a narrow component if the Λ_c^+ is from the decay of the $\Lambda_c(2625)^+$, and there is a broad component if the Λ_c^+ is from the e^+e^- collision and matched with the π pair coming from the $\Lambda_c(2625)^+$. The separated one-dimensional and two-dimensional (2D) signal shape components are displayed in the Fig. 5 and Fig. 6, and the combined shapes are shown in Figs. 4(c) to 4(f).

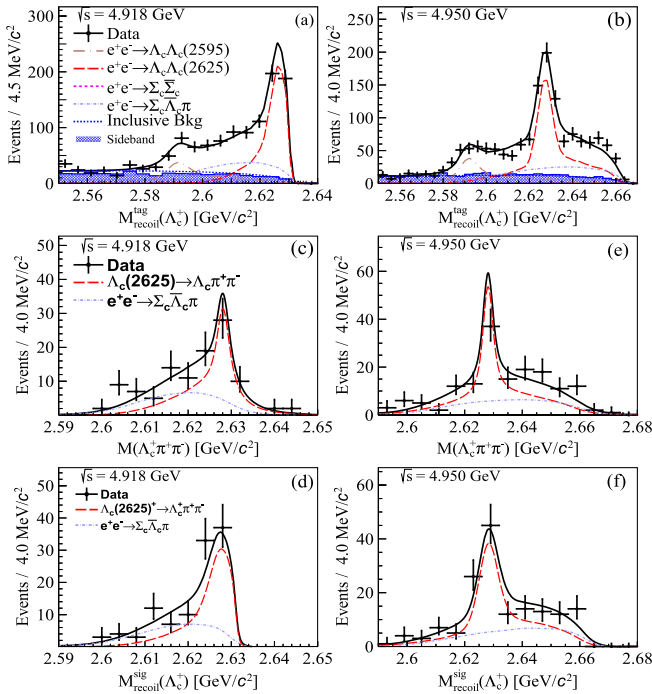


FIG. 4. The distributions of $M_{\text{recoil}}^{\text{sig}}(\Lambda_c^+)$ at (a) $\sqrt{s} = 4.918$ GeV and (b) 4.950 GeV, and distributions of (c), (d) $M(\Lambda_c^+\pi^+\pi^-)$, and (e), (f) $M_{\text{recoil}}^{\text{sig}}(\Lambda_c^+)$, with all the selection criteria for $\Lambda_c^+\pi^+\pi^-$. The black points with error bars are data, the solid curves represent the fit results, and the dashed ones describe individual components including both signal and backgrounds.

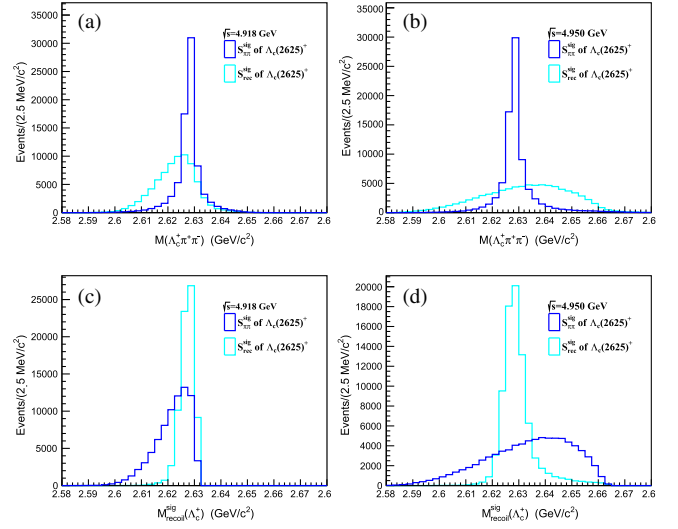


FIG. 5. The one-dimensional distributions (a) and (b) $M(\Lambda_c^+\pi^+\pi^-)$ (c) and (d) $M_{\text{recoil}}^{\text{sig}}(\Lambda_c^+)$ of signal MC $S_{\pi\pi}^{\text{sig}}$ and $S_{\text{rec}}^{\text{sig}}$ for $\sqrt{s} = 4.918$ (left) and 4.950 GeV (right).

V. BACKGROUND ANALYSES

As shown in Figs. 4(a) and 4(b), the remaining contamination of the $e^+e^- \rightarrow \bar{\Lambda}_c^-\Lambda_c(2595)^+$ and $\bar{\Lambda}_c^-\Lambda_c(2625)^+$ candidates is from inclusive background, $e^+e^- \rightarrow \Sigma_c\bar{\Sigma}_c$ and $\Sigma_c\bar{\Lambda}_c\pi$. The inclusive background events are smoothly distributed under the $\Lambda_c(2595)^+$ and $\Lambda_c(2625)^+$ peaks, and estimated with sideband events $M(\Lambda_c^+) \in (2.18, 2.25)$ and $(2.32, 2.39)$ GeV/ c^2 . Σ_c decays to $\Lambda_c^+\pi$ dominantly, but the mass distributions from the processes $e^+e^- \rightarrow \Sigma_c\bar{\Sigma}_c$ and $\Sigma_c\bar{\Lambda}_c\pi$ can be distinguished from those of $e^+e^- \rightarrow \Lambda_c^+\bar{\Lambda}_c(2595)^-$ and $\Lambda_c^+\bar{\Lambda}_c(2625)^-$. In Figs. 4(c) to 4(f), the

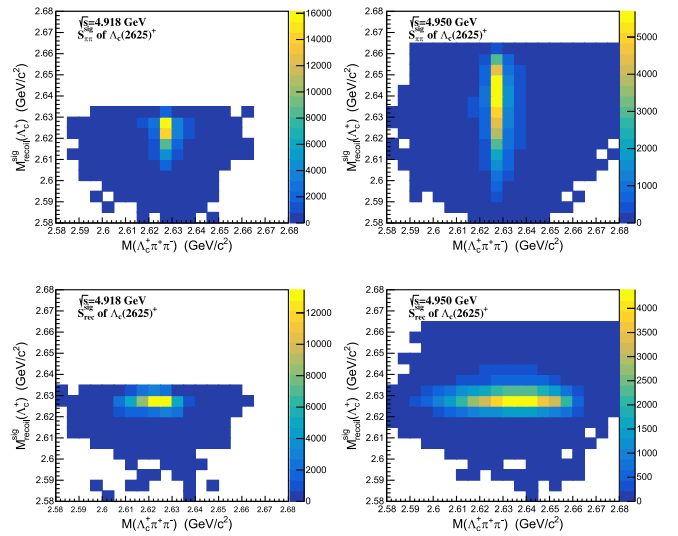


FIG. 6. The 2D distributions $M(\Lambda_c^+\pi^+\pi^-)$ versus $M_{\text{recoil}}^{\text{sig}}(\Lambda_c^+)$ of signal MC $S_{\pi\pi}^{\text{sig}}$ and $S_{\text{rec}}^{\text{sig}}$ for $\sqrt{s} = 4.918$ (left) and 4.950 GeV (right).

inclusive background contribution is highly suppressed and is negligible. The remaining contamination comes from $e^+e^- \rightarrow \Sigma_c \bar{\Sigma}_c$ and $\Sigma_c \bar{\Lambda}_c^- \pi$ since they have the same final states as the signal.

VI. BRANCHING FRACTION MEASUREMENT

The total yields N_{tag} for $\Lambda_c(2595)^+$ or $\Lambda_c(2625)^+$ are obtained by performing an unbinned maximum likelihood fit (fit_{tag}) to the distributions of $M_{\text{recoil}}^{\text{tag}}(\Lambda_c^+)$ for each energy point. The candidates for $\Lambda_c(2595)^+$ and $\Lambda_c(2625)^+$ are from both S_{bachelor} and S_{daughter} (as Fig. 1). The two contributions have the same cross section but different detection efficiencies ϵ_{tag}^i , and their shapes are obtained with MC simulation. In these MC samples, the decays of $\Lambda_c(2595)^+$ and $\Lambda_c(2625)^+$ are modeled based on the information in the PDG [2], and both of them decay into $\Lambda_c^+ \pi^+ \pi^-$ and $\Lambda_c^+ \pi^0 \pi^0$ final states, where the decay of $\Lambda_c(2595)^+$ via $\Sigma_c \pi$ has a rate of 73%. To account for the resolution difference between data and MC simulation, the narrow S_{bachelor} signal shapes are convoluted with Gaussian functions, which are shared between the two resonances due to the limited sample sizes at individual energy points. The width of the convolution Gaussian, a free parameter, actually is the resolution difference between data and MC simulation. The signal shapes of S_{bachelor} and the broad S_{daughter} are merged together in the fit, which are shown in Figs. 4(a) and 4(b). The inclusive background distributions are modeled by ARGUS functions [33] with the fixed parameters determined by fitting the sideband events. The magnitudes of the inclusive background background are free in the fit_{tag} . The backgrounds from $e^+e^- \rightarrow \Sigma_c \bar{\Sigma}_c$ and $\Sigma_c \bar{\Lambda}_c^- \pi$ are taken into account in the fit, shapes of which are derived from MC simulations and yields are determined in the fit_{tag} . The resultant fit curves are depicted in Figs. 4(a) and 4(b). The significances of the $\Lambda_c(2595)^+$ signal in the

recoil mass distributions from the tagged Λ_c^+ are 5.27σ and 8.3σ at $\sqrt{s} = 4.918$ and 4.950 GeV, respectively. The corresponding values for the $\Lambda_c(2625)^+$ signal are 12.7σ and 14.0σ .

The signal yields N_{sig} of $\Lambda_c(2595)^+$ or $\Lambda_c(2625)^+ \rightarrow \Lambda_c^+ \pi^+ \pi^-$ are obtained by simultaneous 2D unbinned maximum likelihood fits (fit_{sig}) to the distributions of $M(\Lambda_c^+ \pi^+ \pi^-)$ and $M_{\text{recoil}}^{\text{sig}}(\Lambda_c^+)$ in the Λ_c^+ signal regions of the two c.m. energies, which have the same branching fraction. The 2D signal shapes of $\Lambda_c(2625)^+ \rightarrow \Lambda_c^+ \pi^+ \pi^-$ and those from $e^+e^- \rightarrow \Sigma_c \bar{\Lambda}_c^- \pi$ background are modeled by MC simulations, with the magnitudes free in the fit_{sig} . The 2D signal MC distributions are shown in Fig. 6. Because the decay $\Lambda_c(2595)^+ \rightarrow \Lambda_c^+ \pi^+ \pi^-$ is not observed significantly, as shown in Figs 4(c) to 4(f), its contribution is not considered in the nominal fit_{sig} . Also, $e^+e^- \rightarrow \Sigma_c \bar{\Sigma}_c$ is not included, since its contribution is negligible according to the result of fit_{tag} . The resulting fit curves are shown in Figs. 4(c) to 4(f). The statistical significance of $\Lambda_c(2625)^+ \rightarrow \Lambda_c^+ \pi^+ \pi^-$ is 11.9σ , as calculated with the change of the likelihood values between the fits with and without the signal component, and accounting for the change in the number of degrees of freedom.

Finally, we combine the fit_{tag} and fit_{sig} simultaneously with N_{tag} and efficiency ($N_{\text{sig}}/N_{\text{tag}}$) as parameters according to Eq. (1) to directly obtain the value of the branching fraction in the fit. The yields of N_{tag} and N_{sig} in the final combined fit are listed in Table I. The branching fraction of $\Lambda_c(2625)^+ \rightarrow \Lambda_c^+ \pi^+ \pi^-$ is determined to be $(50.2 \pm 5.7 \pm 3.5)\%$, where the first uncertainty is statistical and the second systematic. Since no significant $\Lambda_c(2595)^+$ signal is observed in the signal process, we calculate the upper limit of the branching fraction of $\Lambda_c(2595)^+ \rightarrow \Lambda_c^+ \pi^+ \pi^-$ based on the method in Ref. [34]. We integrate the likelihood curve as a function of the branching fraction of $\Lambda_c(2595)^+ \rightarrow \Lambda_c^+ \pi^+ \pi^-$ from zero to

TABLE I. The branching fractions of $\Lambda_c(2595)^+$ and $\Lambda_c(2625)^+ \rightarrow \Lambda_c^+ \pi^+ \pi^-$ and the detection efficiencies of ϵ_{tag} and ϵ_{sig} for each reconstruction mode at $\sqrt{s} = 4.918$ (4.950) GeV, where the efficiencies are expressed in percentage. The numbers of events of N_{tag} and N_{sig} combine the three reconstruction modes at $\sqrt{s} = 4.918$ (4.950) GeV.

Λ_c^+ decays		$pK^- \pi^+$	pK_S^0	$\Lambda \pi^+$
$\bar{\Lambda}_c^- \Lambda_c(2625)^+$	$\epsilon_{\text{tag}} / \%$	46.7 (48.4)	50.2 (50.1)	38.4 (39.7)
	$\epsilon_{\text{sig}} / \%$	14.6 (15.1)	16.7 (16.6)	12.8 (12.0)
	N_{tag}		438.3 ± 30.0 (666.0 ± 51.0)	
	N_{sig}		69.5 ± 7.9 (105.1 ± 11.9)	
	$B / \%$		$50.2 \pm 5.7 \pm 3.5$	
$\bar{\Lambda}_c^- \Lambda_c(2595)^+$	$\epsilon_{\text{tag}} / \%$	48.5 (48.8)	49.9 (49.0)	38.5 (37.8)
	$\epsilon_{\text{sig}} / \%$	2.0 (2.5)	2.2 (2.7)	1.6 (2.1)
	N_{tag}		159.3 ± 33.7 (214.1 ± 29.7)	
	N_{sig}		<5.5 (9.6)	
	$B / \%$		<85.0	

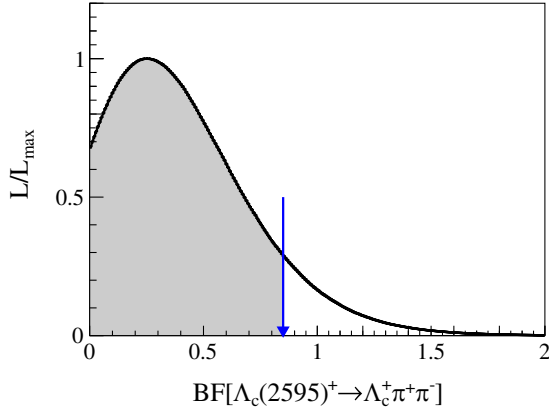


FIG. 7. Likelihood distributions over the branching fraction of $\Lambda_c(2595)^+$. The black solid curve is the scan result with systematic uncertainties. The blue arrow indicates the upper limit of the branching fraction at 90% C.L.

90% of the total area, and the upper limit on its branching fraction at the 90% confidence level is 85.0% (see Fig. 7), where both additive and multiplicative uncertainties are considered.

VII. SYSTEMATIC UNCERTAINTY

The systematic uncertainties in the branching fraction measurement are associated with the π^\pm tracking and PID efficiencies, the signal modeling, the requirement of ΔM , and the fit strategy. In the measurement of absolute branching fractions, the selection criteria of the “tagged Λ_c^+ ” affect both N_{tag} and N_{sig} in Eq. (1). Therefore, the systematic uncertainties of detection efficiency and \mathcal{B}_{tag} cancel.

The uncertainties associated with the π^\pm tracking and PID efficiencies are calculated to be 3.5%, by using the control sample of $J/\psi \rightarrow p\bar{p}\pi^+\pi^-$ [35]. The uncertainty due to the requirement on ΔM is 0.1%, which has been estimated by studies of the resolution difference between data and MC simulation on the ΔM distribution. The uncertainty in the signal MC modeling is 2.2%, determined by taking into account potential Σ_c intermediate resonances to the signal MC samples. The uncertainties due to the fit strategy are 5.4%, including those from the wrong match components of $\Lambda_c^+\pi^+\pi^-$, the modeling of $e^+e^- \rightarrow \Sigma_c\bar{\Lambda}_c^-\pi$ by varying the ratio of production cross sections of $e^+e^- \rightarrow \Sigma_c^0\bar{\Lambda}_c^-\pi^+$, $\Sigma_c^+\bar{\Lambda}_c^-\pi^0$ and $\Sigma_c^{++}\bar{\Lambda}_c^-\pi^-$, and consideration of the potential background $e^+e^- \rightarrow \Lambda_c^+\bar{\Lambda}_c^-\pi^+\pi^-$ by replacing the component $e^+e^- \rightarrow \Sigma_c^0\bar{\Lambda}_c^-\pi^+$ by it in the fit. All other sources from, e.g., the MC statistics, the fitted ranges and the background shapes in fit_{tag} are found to be negligible. Assuming all sources are uncorrelated, the total uncertainties are determined by the quadratic sum of the individual values, which result in 6.8% for the decays $\Lambda_c(2595)^+$ and $\Lambda_c(2625)^+ \rightarrow \Lambda_c^+\pi^+\pi^-$. All

TABLE II. The summary of the systematic uncertainties.

Source	Uncertainty
π^\pm tracking and PID efficiencies	3.5%
Requirement on ΔM	0.1%
Signal MC modeling	2.4%
Fit strategy	5.4%
Total	6.9%

the sources of systematic uncertainties are summarized in Table II.

VIII. SUMMARY

In summary, the branching fraction of the strong decay $\Lambda_c(2625)^+ \rightarrow \Lambda_c^+\pi^+\pi^-$ and upper limit for $\Lambda_c(2595)^+ \rightarrow \Lambda_c^+\pi^+\pi^-$ were determined for the first time, in a model-independent approach by using the 368.5 pb^{-1} of e^+e^- data collected at $\sqrt{s} = 4.918$ and 4.950 GeV with the BESIII detector. The absolute branching fraction of $\Lambda_c(2625)^+ \rightarrow \Lambda_c^+\pi^+\pi^-$ was measured to be $(50.2 \pm 5.7_{\text{stat}} \pm 3.5_{\text{syst}})\%$. Although the central value of the result is lower than the theoretical prediction of 67% [2], obtained from isospin symmetry, they are consistent taking the uncertainties into account. Our result provides critical experimental input to determine the coupling constants in the HHChPT [6,7]. In addition, the measured absolute branching fraction is also essential to calibrate the relative measurements and guide the search for unknown decays of $\Lambda_c(2625)^+$. No discernible signal of the decay $\Lambda_c(2595)^+ \rightarrow \Lambda_c^+\pi^+\pi^-$ was observed and the upper limit on its branching fraction at the 90% confidence level is 85.0%.

ACKNOWLEDGMENTS

The BESIII Collaboration thanks the staff of BEPCII and the IHEP computing center for their strong support. This work is supported in part by National Key R&D Program of China under Contracts Nos. 2020YFA0406300, 2020YFA0406400; National Natural Science Foundation of China (NSFC) under Contracts Nos. 11635010, 11735014, 11835012, 11935015, 11935016, 11935018, 11961141012, 12025502, 12035009, 12035013, 12061131003, 12192260, 12192261, 12192262, 12192263, 12192264, 12192265, 12221005, 12225509, 12235017, 12005311; the Chinese Academy of Sciences (CAS) Large-Scale Scientific Facility Program; the CAS Center for Excellence in Particle Physics (CCEPP); Joint Large-Scale Scientific Facility Funds of the NSFC and CAS under Contract No. U1832207; CAS Key Research Program of Frontier Sciences under Contracts Nos. QYZDJ-SSW-SLH003, QYZDJ-SSW-SLH040; 100 Talents Program of CAS; The Institute of Nuclear and Particle Physics (INPAC) and Shanghai Key Laboratory for Particle Physics and Cosmology; European Union’s

Horizon 2020 research and innovation programme under Marie Skłodowska-Curie grant agreement under Contract No. 894790; German Research Foundation DFG under Contracts Nos. 455635585, Collaborative Research Center CRC 1044, FOR5327, GRK 2149; Istituto Nazionale di Fisica Nucleare, Italy; Ministry of Development of Turkey under Contract No. DPT2006K-120470; National Research Foundation of Korea under Contract No. NRF-2022R1A2C1092335; National Science and Technology

fund of Mongolia; National Science Research and Innovation Fund (NSRF) via the Program Management Unit for Human Resources & Institutional Development, Research and Innovation of Thailand under Contract No. B16F640076; Polish National Science Centre under Contract No. 2019/35/O/ST2/02907; The Swedish Research Council; The Knut and Alice Wallenberg Foundation, Sweden; U.S. Department of Energy under Contract No. DE-FG02-05ER41374.

-
- [1] H. Y. Cheng, *Chin. J. Phys.* **78**, 324 (2022).
 [2] R. L. Workman *et al.* (Particle Data Group), *Prog. Theor. Exp. Phys.* **2022**, 083C01 (2022).
 [3] K. W. Edwards *et al.* (CLEO Collaboration), *Phys. Rev. Lett.* **74**, 3331 (1995).
 [4] H. Albrecht *et al.* (ARGUS Collaboration), *Phys. Lett. B* **402**, 207 (1997).
 [5] D. Wang *et al.* (Belle Collaboration), *Phys. Rev. D* **107**, 032008 (2023).
 [6] H. Y. Cheng and C. K. C., *Phys. Rev. D* **75**, 014006 (2007).
 [7] H. Y. Cheng and C. K. C., *Phys. Rev. D* **92**, 074014 (2015).
 [8] T. M. Yan, H. Y. Cheng, C. Y. Cheung, G. L. Lin, Y. C. Lin, and H. L. Yu, *Phys. Rev. D* **46**, 1148 (1992).
 [9] D. Pirjol and T. M. Yan, *Phys. Rev. D* **56**, 5483 (1997).
 [10] A. E. Blechman and A. F. Falk and D. Pirjol, and J. M. Yelton, *Phys. Rev. D* **67**, 074033 (2003).
 [11] P. L. Frabetti *et al.* (E687 Collaboration), *Phys. Rev. Lett.* **72**, 961 (1994).
 [12] P. L. Frabetti *et al.* (E687 Collaboration), *Phys. Lett. B* **365**, 461 (1996).
 [13] H. Albrecht *et al.* (ARGUS Collaboration), *Phys. Lett. B* **317**, 227 (1993).
 [14] T. Aaltonen *et al.* (CDF Collaboration), *Phys. Rev. D* **84**, 012003 (2011).
 [15] A. J. Arifi, H. Nagahiro, and A. Hosaka, *Phys. Rev. D* **95**, 114018 (2017).
 [16] J. X. Lu, Y. Zhou, H. X. Chen, J. J. Xie, and L. S. Geng, *Phys. Rev. D* **92**, 014036 (2015).
 [17] J. Nieves and R. Pavao, *Phys. Rev. D* **101**, 014018 (2020).
 [18] Q. Zhang, X. H. Hu, B. R. He, and J. L. Ping, *Eur. Phys. J. C* **81**, 224 (2021).
 [19] K. Moriya *et al.* (CLAS Collaboration), *Phys. Rev. Lett.* **112**, 082004 (2014).
 [20] H. Kamano, S. X. Nakamura, T.-S. H. Lee, and T. Sato, *Phys. Rev. C* **92**, 025205 (2015).
 [21] B.-C. Ke, J. Koponen, H. B. Li, and Y. H. Zheng, *Annu. Rev. Nucl. Part. Sci.* **73**, 285 (2023).
 [22] M. Ablikim *et al.* (BESIII Collaboration), *Chin. Phys. C* **46**, 113003 (2022).
 [23] M. Ablikim *et al.* (BESIII Collaboration), *Nucl. Instrum. Methods Phys. Res., Sect. A* **614**, 345 (2010).
 [24] S. Agostinelli *et al.* (GEANT4 Collaboration), *Nucl. Instrum. Methods Phys. Res., Sect. A* **506**, 250 (2003).
 [25] K. X. Huang *et al.*, *Nucl. Sci. Tech.* **33**, 142 (2022).
 [26] D. J. Lange, *Nucl. Instrum. Methods Phys. Res., Sect. A* **462**, 152 (2001).
 [27] R. G. Ping, *Chin. Phys. C* **32**, 599 (2008).
 [28] J. C. Chen, G. S. Huang, X. R. Qi, D. H. Zhang, and Y. S. Zhu, *Phys. Rev. D* **62**, 034003 (2000).
 [29] Y. L. Yang, R. G. Ping, and H. Chen, *Phys. Rev. Lett.* **31**, 061301 (2014).
 [30] E. R. Was, *Phys. Lett. B* **303**, 163 (1993).
 [31] M. Ablikim *et al.* (BESIII Collaboration), *arXiv*: 2312.08414.
 [32] S. Jadach, B. F. L. Ward, and Z. Was, *Phys. Rev. D* **63**, 113009 (2001).
 [33] H. Albrecht *et al.* (ARGUS Collaboration), *Phys. Lett. B* **241**, 278 (1990).
 [34] K. Stenson, *arXiv physics/0605236*.
 [35] M. Ablikim *et al.* (BESIII Collaboration), *Phys. Rev. Lett.* **131**, 191901 (2023).

M. Ablikim,¹ M. N. Achasov,^{4,b} P. Adlarson,⁷⁵ X. C. Ai,⁸⁰ R. Aliberti,³⁵ A. Amoroso,^{74a,74c} M. R. An,³⁹ Q. An,^{71,58} Y. Bai,⁵⁷ O. Bakina,³⁶ I. Balossino,^{29a} Y. Ban,^{46,g} H.-R. Bao,⁶³ V. Batozskaya,^{1,44} K. Begzsuren,³² N. Berger,³⁵ M. Berlowski,⁴⁴ M. Bertani,^{28a} D. Bettoni,^{29a} F. Bianchi,^{74a,74c} E. Bianco,^{74a,74c} A. Bortone,^{74a,74c} I. Boyko,³⁶ R. A. Briere,⁵ A. Brueggemann,⁶⁸ H. Cai,⁷⁶ X. Cai,^{1,58} A. Calcaterra,^{28a} G. F. Cao,^{1,63} N. Cao,^{1,63} S. A. Cetin,^{62a} J. F. Chang,^{1,58} W. L. Chang,^{1,63} G. R. Che,⁴³ G. Chelkov,^{36,a} C. Chen,⁴³ Chao Chen,⁵⁵ G. Chen,¹ H. S. Chen,^{1,63} M. L. Chen,^{1,58,63} S. J. Chen,⁴² S. L. Chen,⁴⁵ S. M. Chen,⁶¹ T. Chen,^{1,63} X. R. Chen,^{31,63} X. T. Chen,^{1,63} Y. B. Chen,^{1,58} Y. Q. Chen,³⁴ Z. J. Chen,^{25,h} S. K. Choi,¹⁰ X. Chu,⁴³ G. Cibinetto,^{29a} S. C. Coen,³ F. Cossio,^{74c} J. J. Cui,⁵⁰ H. L. Dai,^{1,58} J. P. Dai,⁷⁸

A. Dbeysyi,¹⁸ R. E. de Boer,³ D. Dedovich,³⁶ Z. Y. Deng,¹ A. Denig,³⁵ I. Denysenko,³⁶ M. Destefanis,^{74a,74c} F. De Mori,^{74a,74c}
 B. Ding,^{66,1} X. X. Ding,^{46,g} Y. Ding,³⁴ Y. Ding,⁴⁰ J. Dong,^{1,58} L. Y. Dong,^{1,63} M. Y. Dong,^{1,58,63} X. Dong,⁷⁶ M. C. Du,¹
 S. X. Du,⁸⁰ Z. H. Duan,⁴² P. Egorov,^{36,a} Y. H. Fan,⁴⁵ J. Fang,^{1,58} S. S. Fang,^{1,63} W. X. Fang,¹ Y. Fang,¹ Y. Q. Fang,^{1,58}
 R. Farinelli,^{29a} L. Fava,^{74b,74c} F. Feldbauer,³ G. Felici,^{28a} C. Q. Feng,^{71,58} J. H. Feng,⁵⁹ Y. T. Feng,^{71,58} K. Fischer,⁶⁹
 M. Fritsch,³ C. D. Fu,¹ J. L. Fu,⁶³ Y. W. Fu,¹ H. Gao,⁶³ Y. N. Gao,^{46,g} Yang Gao,^{71,58} S. Garbolino,^{74c} I. Garzia,^{29a,29b}
 P. T. Ge,⁷⁶ Z. W. Ge,⁴² C. Geng,⁵⁹ E. M. Gersabeck,⁶⁷ A. Gilman,⁶⁹ K. Goetzen,¹³ L. Gong,⁴⁰ W. X. Gong,^{1,58} W. Gradl,³⁵
 S. Gramigna,^{29a,29b} M. Greco,^{74a,74c} M. H. Gu,^{1,58} Y. T. Gu,¹⁵ C. Y. Guan,^{1,63} Z. L. Guan,²² A. Q. Guo,^{31,63} L. B. Guo,⁴¹
 M. J. Guo,⁵⁰ R. P. Guo,⁴⁹ Y. P. Guo,^{12,f} A. Guskov,^{36,a} J. Gutierrez,²⁷ K. L. Han,⁶³ T. T. Han,¹ W. Y. Han,³⁹ X. Q. Hao,¹⁹
 F. A. Harris,⁶⁵ K. K. He,⁵⁵ K. L. He,^{1,63} F. H. H. Heinsius,³ C. H. Heinz,³⁵ Y. K. Heng,^{1,58,63} C. Herold,⁶⁰ T. Holtmann,³
 P. C. Hong,^{12,f} G. Y. Hou,^{1,63} X. T. Hou,^{1,63} Y. R. Hou,⁶³ Z. L. Hou,¹ B. Y. Hu,⁵⁹ H. M. Hu,^{1,63} J. F. Hu,^{56,i} T. Hu,^{1,58,63} Y. Hu,¹
 G. S. Huang,^{71,58} K. X. Huang,⁵⁹ L. Q. Huang,^{31,63} X. T. Huang,⁵⁰ Y. P. Huang,¹ T. Hussain,⁷³ N. Hüsken,^{27,35}
 N. in der Wiesche,⁶⁸ M. Irshad,^{71,58} J. Jackson,²⁷ S. Jaeger,³ S. Janchiv,³² J. H. Jeong,¹⁰ Q. Ji,¹ Q. P. Ji,¹⁹ X. B. Ji,^{1,63}
 X. L. Ji,^{1,58} Y. Y. Ji,⁵⁰ X. Q. Jia,⁵⁰ Z. K. Jia,^{71,58} H. B. Jiang,⁷⁶ P. C. Jiang,^{46,g} S. S. Jiang,³⁹ T. J. Jiang,¹⁶ X. S. Jiang,^{1,58,63}
 Y. Jiang,⁶³ J. B. Jiao,⁵⁰ Z. Jiao,²³ S. Jin,⁴² Y. Jin,⁶⁶ M. Q. Jing,^{1,63} X. M. Jing,⁶³ T. Johansson,⁷⁵ X. K.,¹ S. Kabana,³³
 N. Kalantar-Nayestanaki,⁶⁴ X. L. Kang,⁹ X. S. Kang,⁴⁰ M. Kavatsyuk,⁶⁴ B. C. Ke,⁸⁰ V. Khachatryan,²⁷ A. Khoukaz,⁶⁸
 R. Kiuchi,¹ O. B. Kolcu,^{62a} B. Kopf,³ M. Kuessner,³ A. Kupsc,^{44,75} W. Kühn,³⁷ J. J. Lane,⁶⁷ P. Larin,¹⁸ L. Lavezzi,^{74a,74c}
 T. T. Lei,^{71,58} Z. H. Lei,^{71,58} H. Leithoff,³⁵ M. Lellmann,³⁵ T. Lenz,³⁵ C. Li,⁴³ C. Li,⁴⁷ C. H. Li,³⁹ Cheng Li,^{71,58} D. M. Li,⁸⁰
 F. Li,^{1,58} G. Li,¹ H. Li,^{71,58} H. B. Li,^{1,63} H. J. Li,¹⁹ H. N. Li,^{56,i} Hui Li,⁴³ J. R. Li,⁶¹ J. S. Li,⁵⁹ J. W. Li,⁵⁰ Ke Li,¹ L. J. Li,^{1,63}
 L. K. Li,¹ Lei Li,⁴⁸ M. H. Li,⁴³ P. R. Li,^{38,k} Q. X. Li,⁵⁰ S. X. Li,¹² T. Li,⁵⁰ W. D. Li,^{1,63} W. G. Li,¹ X. H. Li,^{71,58} X. L. Li,⁵⁰
 Xiaoyu Li,^{1,63} Y. G. Li,^{46,g} Z. J. Li,⁵⁹ Z. X. Li,¹⁵ C. Liang,⁴² H. Liang,^{71,58} H. Liang,^{1,63} Y. F. Liang,⁵⁴ Y. T. Liang,^{31,63}
 G. R. Liao,¹⁴ L. Z. Liao,⁵⁰ Y. P. Liao,^{1,63} J. Libby,²⁶ A. Limphirat,⁶⁰ D. X. Lin,^{31,63} T. Lin,¹ B. J. Liu,¹ B. X. Liu,⁷⁶ C. Liu,³⁴
 C. X. Liu,¹ F. H. Liu,⁵³ Fang Liu,¹ Feng Liu,⁶ G. M. Liu,^{56,i} H. Liu,^{38,j,k} H. B. Liu,¹⁵ H. M. Liu,^{1,63} Huanhuan Liu,¹
 Huihui Liu,²¹ J. B. Liu,^{71,58} J. Y. Liu,^{1,63} K. Liu,^{38,j,k} K. Y. Liu,⁴⁰ Ke Liu,²² L. Liu,^{71,58} L. C. Liu,⁴³ Lu Liu,⁴³ M. H. Liu,^{12,f}
 P. L. Liu,¹ Q. Liu,⁶³ S. B. Liu,^{71,58} T. Liu,^{12,f} W. K. Liu,⁴³ W. M. Liu,^{71,58} X. Liu,^{38,j,k} Y. Liu,^{38,j,k} Y. Liu,⁸⁰ Y. B. Liu,⁴³
 Z. A. Liu,^{1,58,63} Z. Q. Liu,⁵⁰ X. C. Lou,^{1,58,63} F. X. Lu,⁵⁹ H. J. Lu,²³ J. G. Lu,^{1,58} X. L. Lu,¹ Y. Lu,⁷ Y. P. Lu,^{1,58} Z. H. Lu,^{1,63}
 C. L. Luo,⁴¹ M. X. Luo,⁷⁹ T. Luo,^{12,f} X. L. Luo,^{1,58} X. R. Lyu,⁶³ Y. F. Lyu,⁴³ F. C. Ma,⁴⁰ H. Ma,⁷⁸ H. L. Ma,¹ J. L. Ma,^{1,63}
 L. L. Ma,⁵⁰ M. M. Ma,^{1,63} Q. M. Ma,¹ R. Q. Ma,^{1,63} X. Y. Ma,^{1,58} Y. Ma,^{46,g} Y. M. Ma,³¹ F. E. Maas,¹⁸ M. Maggiora,^{74a,74c}
 S. Malde,⁶⁹ A. Mangoni,^{28b} Y. J. Mao,^{46,g} Z. P. Mao,¹ S. Marcello,^{74a,74c} Z. X. Meng,⁶⁶ J. G. Messchendorp,^{13,64}
 G. Mezzadri,^{29a} H. Miao,^{1,63} T. J. Min,⁴² R. E. Mitchell,²⁷ X. H. Mo,^{1,58,63} B. Moses,²⁷ N. Yu. Muchnoi,^{4,b} J. Muskalla,³⁵
 Y. Nefedov,³⁶ F. Nerling,^{18,d} I. B. Nikolaev,^{4,b} Z. Ning,^{1,58} S. Nisar,^{11,1} Q. L. Niu,^{38,j,k} W. D. Niu,⁵⁵ Y. Niu,⁵⁰ S. L. Olsen,⁶³
 Q. Ouyang,^{1,58,63} S. Pacetti,^{28b,28c} X. Pan,⁵⁵ Y. Pan,⁵⁷ A. Pathak,³⁴ P. Patteri,^{28a} Y. P. Pei,^{71,58} M. Pelizaeus,³ H. P. Peng,^{71,58}
 Y. Y. Peng,^{38,j,k} K. Peters,^{13,d} J. L. Ping,⁴¹ R. G. Ping,^{1,63} S. Plura,³⁵ V. Prasad,³³ F. Z. Qi,¹ H. Qi,^{71,58} H. R. Qi,⁶¹ M. Qi,⁴²
 T. Y. Qi,^{12,f} S. Qian,^{1,58} W. B. Qian,⁶³ C. F. Qiao,⁶³ J. J. Qin,⁷² L. Q. Qin,¹⁴ X. S. Qin,⁵⁰ Z. H. Qin,^{1,58} J. F. Qiu,¹ S. Q. Qu,⁶¹
 C. F. Redmer,³⁵ K. J. Ren,³⁹ A. Rivetti,^{74c} M. Rolo,^{74c} G. Rong,^{1,63} Ch. Rosner,¹⁸ S. N. Ruan,⁴³ N. Salone,⁴⁴ A. Sarantsev,^{36,c}
 Y. Schelhaas,³⁵ K. Schoenning,⁷⁵ M. Scodreggio,^{29a,29b} K. Y. Shan,^{12,f} W. Shan,²⁴ X. Y. Shan,^{71,58} J. F. Shangguan,⁵⁵
 L. G. Shao,^{1,63} M. Shao,^{71,58} C. P. Shen,^{12,f} H. F. Shen,^{1,63} W. H. Shen,⁶³ X. Y. Shen,^{1,63} B. A. Shi,⁶³ H. C. Shi,^{71,58} J. L. Shi,¹²
 J. Y. Shi,¹ Q. Q. Shi,⁵⁵ R. S. Shi,^{1,63} X. Shi,^{1,58} J. J. Song,¹⁹ T. Z. Song,⁵⁹ W. M. Song,^{34,1} Y. J. Song,¹² S. Sosio,^{74a,74c}
 S. Spataro,^{74a,74c} F. Stieler,³⁵ Y. J. Su,⁶³ G. B. Sun,⁷⁶ G. X. Sun,¹ H. Sun,⁶³ H. K. Sun,¹ J. F. Sun,¹⁹ K. Sun,⁶¹ L. Sun,⁷⁶
 S. S. Sun,^{1,63} T. Sun,^{51,e} W. Y. Sun,³⁴ Y. Sun,⁹ Y. J. Sun,^{71,58} Y. Z. Sun,¹ Z. T. Sun,⁵⁰ Y. X. Tan,^{71,58} C. J. Tang,⁵⁴ G. Y. Tang,¹
 J. Tang,⁵⁹ Y. A. Tang,⁷⁶ L. Y. Tao,⁷² Q. T. Tao,^{25,h} M. Tat,⁶⁹ J. X. Teng,^{71,58} V. Thoren,⁷⁵ W. H. Tian,⁵² W. H. Tian,⁵⁹
 Y. Tian,^{31,63} Z. F. Tian,⁷⁶ I. Uman,^{62b} Y. Wan,⁵⁵ S. J. Wang,⁵⁰ B. Wang,¹ B. L. Wang,⁶³ Bo Wang,^{71,58} C. W. Wang,⁴²
 D. Y. Wang,^{46,g} F. Wang,⁷² H. J. Wang,^{38,j,k} J. P. Wang,⁵⁰ K. Wang,^{1,58} L. L. Wang,¹ M. Wang,⁵⁰ Meng Wang,^{1,63}
 N. Y. Wang,⁶³ S. Wang,^{12,f} S. Wang,^{38,j,k} T. Wang,^{12,f} T. J. Wang,⁴³ W. Wang,⁵⁹ W. Wang,⁷² W. P. Wang,^{71,58} X. Wang,^{46,g}
 X. F. Wang,^{38,j,k} X. J. Wang,³⁹ X. L. Wang,^{12,f} Y. Wang,⁶¹ Y. D. Wang,⁴⁵ Y. F. Wang,^{1,58,63} Y. L. Wang,¹⁹ Y. N. Wang,⁴⁵
 Y. Q. Wang,¹ Yaqian Wang,^{17,1} Yi Wang,⁶¹ Z. Wang,^{1,58} Z. L. Wang,⁷² Z. Y. Wang,^{1,63} Ziyi Wang,⁶³ D. Wei,⁷⁰ D. H. Wei,¹⁴
 F. Weidner,⁶⁸ S. P. Wen,¹ C. W. Wenzel,³ U. Wiedner,³ G. Wilkinson,⁶⁹ M. Wolke,⁷⁵ L. Wollenberg,³ C. Wu,³⁹ J. F. Wu,^{1,8}
 L. H. Wu,¹ L. J. Wu,^{1,63} X. Wu,^{12,f} X. H. Wu,³⁴ Y. Wu,⁷¹ Y. H. Wu,⁵⁵ Y. J. Wu,³¹ Z. Wu,^{1,58} L. Xia,^{71,58} X. M. Xian,³⁹
 T. Xiang,^{46,g} D. Xiao,^{38,j,k} G. Y. Xiao,⁴² S. Y. Xiao,¹ Y. L. Xiao,^{12,f} Z. J. Xiao,⁴¹ C. Xie,⁴² X. H. Xie,^{46,g} Y. Xie,⁵⁰
 Y. G. Xie,^{1,58} Y. H. Xie,⁶ Z. P. Xie,^{71,58} T. Y. Xing,^{1,63} C. F. Xu,^{1,63} C. J. Xu,⁵⁹ G. F. Xu,¹ H. Y. Xu,⁶⁶ Q. J. Xu,¹⁶ Q. N. Xu,³⁰

W. Xu,¹ W. L. Xu,⁶⁶ X. P. Xu,⁵⁵ Y. C. Xu,⁷⁷ Z. P. Xu,⁴² Z. S. Xu,⁶³ F. Yan,^{12,f} L. Yan,^{12,f} W. B. Yan,^{71,58} W. C. Yan,⁸⁰
 X. Q. Yan,¹ H. J. Yang,^{51,e} H. L. Yang,³⁴ H. X. Yang,¹ Tao Yang,¹ Y. Yang,^{12,f} Y. F. Yang,⁴³ Y. X. Yang,^{1,63} Yifan Yang,^{1,63}
 Z. W. Yang,^{38,j,k} Z. P. Yao,⁵⁰ M. Ye,^{1,58} M. H. Ye,⁸ J. H. Yin,¹ Z. Y. You,⁵⁹ B. X. Yu,^{1,58,63} C. X. Yu,⁴³ G. Yu,^{1,63} J. S. Yu,^{25,h}
 T. Yu,⁷² X. D. Yu,^{46,g} C. Z. Yuan,^{1,63} L. Yuan,² S. C. Yuan,¹ Y. Yuan,^{1,63} Z. Y. Yuan,⁵⁹ C. X. Yue,³⁹ A. A. Zafar,⁷³
 F. R. Zeng,⁵⁰ S. H. Zeng,⁷² X. Zeng,^{12,f} Y. Zeng,^{25,h} Y. J. Zeng,^{1,63} X. Y. Zhai,³⁴ Y. C. Zhai,⁵⁰ Y. H. Zhan,⁵⁹ A. Q. Zhang,^{1,63}
 B. L. Zhang,^{1,63} B. X. Zhang,¹ D. H. Zhang,⁴³ G. Y. Zhang,¹⁹ H. Zhang,⁷¹ H. C. Zhang,^{1,58,63} H. H. Zhang,⁵⁹ H. H. Zhang,³⁴
 H. Q. Zhang,^{1,58,63} H. Y. Zhang,^{1,58} J. Zhang,⁸⁰ J. Zhang,⁵⁹ J. J. Zhang,⁵² J. L. Zhang,²⁰ J. Q. Zhang,⁴¹ J. W. Zhang,^{1,58,63}
 J. X. Zhang,^{38,j,k} J. Y. Zhang,¹ J. Z. Zhang,^{1,63} Jianyu Zhang,⁶³ L. M. Zhang,⁶¹ L. Q. Zhang,⁵⁹ Lei Zhang,⁴² P. Zhang,^{1,63}
 Q. Y. Zhang,^{39,80} Shuihan Zhang,^{1,63} Shulei Zhang,^{25,h} X. D. Zhang,⁴⁵ X. M. Zhang,¹ X. Y. Zhang,⁵⁰ Y. Zhang,⁶⁹ Y. Zhang,⁷²
 Y. T. Zhang,⁸⁰ Y. H. Zhang,^{1,58} Yan Zhang,^{71,58} Yao Zhang,¹ Z. D. Zhang,¹ Z. H. Zhang,¹ Z. L. Zhang,³⁴ Z. Y. Zhang,⁴³
 Z. Y. Zhang,⁷⁶ G. Zhao,¹ J. Y. Zhao,^{1,63} J. Z. Zhao,^{1,58} Lei Zhao,^{71,58} Ling Zhao,¹ M. G. Zhao,⁴³ R. P. Zhao,⁶³ S. J. Zhao,⁸⁰
 Y. B. Zhao,^{1,58} Y. X. Zhao,^{31,63} Z. G. Zhao,^{71,58} A. Zhemchugov,^{36,a} B. Zheng,⁷² J. P. Zheng,^{1,58} W. J. Zheng,^{1,63}
 Y. H. Zheng,⁶³ B. Zhong,⁴¹ X. Zhong,⁵⁹ H. Zhou,⁵⁰ L. P. Zhou,^{1,63} X. Zhou,⁷⁶ X. K. Zhou,⁶ X. R. Zhou,^{71,58} X. Y. Zhou,³⁹
 Y. Z. Zhou,^{12,f} J. Zhu,⁴³ K. Zhu,¹ K. J. Zhu,^{1,58,63} L. Zhu,³⁴ L. X. Zhu,⁶³ S. H. Zhu,⁷⁰ S. Q. Zhu,⁴² T. J. Zhu,^{12,f} W. J. Zhu,^{12,f}
 Y. C. Zhu,^{71,58} Z. A. Zhu,^{1,63} J. H. Zou,¹ and J. Zu^{71,58}

(BESIII Collaboration)

¹*Institute of High Energy Physics, Beijing 100049, People's Republic of China*

²*Beihang University, Beijing 100191, People's Republic of China*

³*Bochum Ruhr-University, D-44780 Bochum, Germany*

⁴*Budker Institute of Nuclear Physics SB RAS (BINP), Novosibirsk 630090, Russia*

⁵*Carnegie Mellon University, Pittsburgh, Pennsylvania 15213, USA*

⁶*Central China Normal University, Wuhan 430079, People's Republic of China*

⁷*Central South University, Changsha 410083, People's Republic of China*

⁸*China Center of Advanced Science and Technology, Beijing 100190, People's Republic of China*

⁹*China University of Geosciences, Wuhan 430074, People's Republic of China*

¹⁰*Chung-Ang University, Seoul, 06974, Republic of Korea*

¹¹*COMSATS University Islamabad, Lahore Campus, Defence Road, Off Raiwind Road, 54000 Lahore, Pakistan*

¹²*Fudan University, Shanghai 200433, People's Republic of China*

¹³*GSI Helmholtzcentre for Heavy Ion Research GmbH, D-64291 Darmstadt, Germany*

¹⁴*Guangxi Normal University, Guilin 541004, People's Republic of China*

¹⁵*Guangxi University, Nanning 530004, People's Republic of China*

¹⁶*Hangzhou Normal University, Hangzhou 310036, People's Republic of China*

¹⁷*Hebei University, Baoding 071002, People's Republic of China*

¹⁸*Helmholtz Institute Mainz, Staudinger Weg 18, D-55099 Mainz, Germany*

¹⁹*Henan Normal University, Xinxiang 453007, People's Republic of China*

²⁰*Henan University, Kaifeng 475004, People's Republic of China*

²¹*Henan University of Science and Technology, Luoyang 471003, People's Republic of China*

²²*Henan University of Technology, Zhengzhou 450001, People's Republic of China*

²³*Huangshan College, Huangshan 245000, People's Republic of China*

²⁴*Hunan Normal University, Changsha 410081, People's Republic of China*

²⁵*Hunan University, Changsha 410082, People's Republic of China*

²⁶*Indian Institute of Technology Madras, Chennai 600036, India*

²⁷*Indiana University, Bloomington, Indiana 47405, USA*

^{28a}*INFN Laboratori Nazionali di Frascati, I-00044, Frascati, Italy*

^{28b}*INFN Sezione di Perugia, I-06100, Perugia, Italy*

^{28c}*University of Perugia, I-06100, Perugia, Italy*

^{29a}*INFN Sezione di Ferrara, I-44122, Ferrara, Italy*

^{29b}*University of Ferrara, I-44122, Ferrara, Italy*

³⁰*Inner Mongolia University, Hohhot 010021, People's Republic of China*

³¹*Institute of Modern Physics, Lanzhou 730000, People's Republic of China*

³²*Institute of Physics and Technology, Peace Avenue 54B, Ulaanbaatar 13330, Mongolia*

³³*Instituto de Alta Investigación, Universidad de Tarapacá, Casilla 7D, Arica 1000000, Chile*

³⁴*Jilin University, Changchun 130012, People's Republic of China*

- ³⁵Johannes Gutenberg University of Mainz, Johann-Joachim-Becher-Weg 45, D-55099 Mainz, Germany
- ³⁶Joint Institute for Nuclear Research, 141980 Dubna, Moscow region, Russia
- ³⁷Justus-Liebig-Universitaet Giessen, II. Physikalisches Institut, Heinrich-Buff-Ring 16, D-35392 Giessen, Germany
- ³⁸Lanzhou University, Lanzhou 730000, People's Republic of China
- ³⁹Liaoning Normal University, Dalian 116029, People's Republic of China
- ⁴⁰Liaoning University, Shenyang 110036, People's Republic of China
- ⁴¹Nanjing Normal University, Nanjing 210023, People's Republic of China
- ⁴²Nanjing University, Nanjing 210093, People's Republic of China
- ⁴³Nankai University, Tianjin 300071, People's Republic of China
- ⁴⁴National Centre for Nuclear Research, Warsaw 02-093, Poland
- ⁴⁵North China Electric Power University, Beijing 102206, People's Republic of China
- ⁴⁶Peking University, Beijing 100871, People's Republic of China
- ⁴⁷Qufu Normal University, Qufu 273165, People's Republic of China
- ⁴⁸Renmin University of China, Beijing 100872, People's Republic of China
- ⁴⁹Shandong Normal University, Jinan 250014, People's Republic of China
- ⁵⁰Shandong University, Jinan 250100, People's Republic of China
- ⁵¹Shanghai Jiao Tong University, Shanghai 200240, People's Republic of China
- ⁵²Shanxi Normal University, Linfen 041004, People's Republic of China
- ⁵³Shanxi University, Taiyuan 030006, People's Republic of China
- ⁵⁴Sichuan University, Chengdu 610064, People's Republic of China
- ⁵⁵Soochow University, Suzhou 215006, People's Republic of China
- ⁵⁶South China Normal University, Guangzhou 510006, People's Republic of China
- ⁵⁷Southeast University, Nanjing 211100, People's Republic of China
- ⁵⁸State Key Laboratory of Particle Detection and Electronics, Beijing 100049, Hefei 230026, People's Republic of China
- ⁵⁹Sun Yat-Sen University, Guangzhou 510275, People's Republic of China
- ⁶⁰Suranaree University of Technology, University Avenue 111, Nakhon Ratchasima 30000, Thailand
- ⁶¹Tsinghua University, Beijing 100084, People's Republic of China
- ^{62a}Turkish Accelerator Center Particle Factory Group, Istinye University, 34010, Istanbul, Turkey
- ^{62b}Near East University, Nicosia, North Cyprus, 99138, Mersin 10, Turkey
- ⁶³University of Chinese Academy of Sciences, Beijing 100049, People's Republic of China
- ⁶⁴University of Groningen, NL-9747 AA Groningen, The Netherlands
- ⁶⁵University of Hawaii, Honolulu, Hawaii 96822, USA
- ⁶⁶University of Jinan, Jinan 250022, People's Republic of China
- ⁶⁷University of Manchester, Oxford Road, Manchester, M13 9PL, United Kingdom
- ⁶⁸University of Muenster, Wilhelm-Klemm-Strasse 9, 48149 Muenster, Germany
- ⁶⁹University of Oxford, Keble Road, Oxford OX13RH, United Kingdom
- ⁷⁰University of Science and Technology Liaoning, Anshan 114051, People's Republic of China
- ⁷¹University of Science and Technology of China, Hefei 230026, People's Republic of China
- ⁷²University of South China, Hengyang 421001, People's Republic of China
- ⁷³University of the Punjab, Lahore-54590, Pakistan
- ^{74a}University of Turin and INFN, University of Turin, I-10125, Turin, Italy
- ^{74b}University of Eastern Piedmont, I-15121, Alessandria, Italy
- ^{74c}INFN, I-10125, Turin, Italy
- ⁷⁵Uppsala University, Box 516, SE-75120 Uppsala, Sweden
- ⁷⁶Wuhan University, Wuhan 430072, People's Republic of China
- ⁷⁷Yantai University, Yantai 264005, People's Republic of China
- ⁷⁸Yunnan University, Kunming 650500, People's Republic of China
- ⁷⁹Zhejiang University, Hangzhou 310027, People's Republic of China
- ⁸⁰Zhengzhou University, Zhengzhou 450001, People's Republic of China

^aAlso at the Moscow Institute of Physics and Technology, Moscow 141700, Russia.

^bAlso at the Novosibirsk State University, Novosibirsk, 630090, Russia.

^cAlso at the NRC "Kurchatov Institute", PNPI, 188300, Gatchina, Russia.

^dAlso at Goethe University Frankfurt, 60323 Frankfurt am Main, Germany.

^eAlso at Key Laboratory for Particle Physics, Astrophysics and Cosmology, Ministry of Education; Shanghai Key Laboratory for Particle Physics and Cosmology; Institute of Nuclear and Particle Physics, Shanghai 200240, People's Republic of China.

^fAlso at Key Laboratory of Nuclear Physics and Ion-beam Application (MOE) and Institute of Modern Physics, Fudan University, Shanghai 200443, People's Republic of China.

^gAlso at State Key Laboratory of Nuclear Physics and Technology, Peking University, Beijing 100871, People's Republic of China.

^hAlso at School of Physics and Electronics, Hunan University, Changsha 410082, China.

ⁱAlso at Guangdong Provincial Key Laboratory of Nuclear Science, Institute of Quantum Matter, South China Normal University, Guangzhou 510006, China.

^jAlso at MOE Frontiers Science Center for Rare Isotopes, Lanzhou University, Lanzhou 730000, People's Republic of China.

^kAlso at Lanzhou Center for Theoretical Physics, Lanzhou University, Lanzhou 730000, People's Republic of China.

^lAlso at the Department of Mathematical Sciences, IBA, Karachi 75270, Pakistan.